Applied Nanoscience (2023) 13:4005–4019
https://doi.org/10.1007/s13204-022-02680-7

ORIGINAL ARTICLE

Synthesis of zeolitic imidazolate framework-8 (ZIF-8) using different solvents for lead and cadmium adsorption

Siti Zu Nurain Ahmad[1,2] · Wan Norharyati Wan Salleh[1,2] · Norhaniza Yusof[1,2] · Mohd Zamri Mohd Yusop[1,3] · Rafidah Hamdan[1,2,3,4] · Ahmad Fauzi Ismail[1,2]

Received: 2 June 2022 / Accepted: 8 October 2022 / Published online: 15 November 2022

Abstract

The current study is focused on the facile synthesis of zeolitic imidazolate framework-8 (ZIF-8) at room temperature using three different solvents: ammonia solution (ZIF-8 (N)), aqueous solution (ZIF-8 (H)), and methanol (ZIF-8 (M)). The ZIF-8s produced have high crystallinity with different sizes and shapes. The morphology of ZIF-8 (H) resembled the mixture of cubic and the rhombic dodecahedron with truncated corners, whereas ZIF-8(M) occurred as the most stable rhombic dodecahedron, and ZIF-8(N) appeared as cubes with truncated corners. ZIF-8 (N) had the largest average particle size of 573 nm, followed by ZIF-8 (H) and ZIF-8 (M) with average sizes of 108 nm and 62 nm, respectively. ZIF-8 (N) showed a rapid Pb(II) and Cd(II) adsorption, within 15 min, while ZIF-8(H) achieved Pb(II) and Cd(II) equilibrium within 240 min, and 300 min for ZIF-8 (M). The adsorption of Pb(II) and Cd(II) is best fitted with the Langmuir isotherm and pseudo-second-order kinetic model. The maximum adsorption capacities for Pb(II) and Cd(II) sorption were 454.55 and 312.50 mg/g for ZIF-8 (H), 434.78 and 277.78 mg/g for ZIF-8 (M), respectively, and 476.19 and 263.16 mg/g for ZIF-8 (N), respectively. All of the prepared ZIF-8s showed a promising competency as adsorbents for the removal of Pb(II) and Cd(II) from an aqueous solution.

Keywords Adsorption · Heavy metals · MOF · Solvent effect · Wastewater treatment · ZIF

Introduction

Over the years, the rapid development and intense growth of industrialization have introduced a large amount of heavy metal effluents which added to the severity of water pollution (Maaloul et al. 2021). The non-biodegradable nature of heavy metals as well as their ability to persist in the aqueous ecosystem is, thus, becoming a threat to human beings and nature (Farouz et al. 2022). Various wastewater treatment technologies have been developed to remove heavy metals from the aqueous solution, for instance, ion exchange (Bezzina et al. 2019), precipitation (Pohl 2020), membrane filtration (Awang et al. 2019), electrochemistry (Xu et al. 2019), photocatalysis (Hernández et al. 2022; Moharana et al. 2021), and adsorption (Ahmed et al. 2017; Awes et al. 2021). Adsorption is one of the most popular choices for heavy metals removal owing to its simplicity and low cost, ease of operation, and insensitivity to harmful and toxic pollutants (Peng et al. 2017). Good adsorbents should have functional groups with high affinity in adsorbing heavy metals, as well as high porosity and large specific surface area for the adsorption sites.

The utilization of nanotechnology in the pursuit of a sustainable environment has been highlighted regularly due to numerous advantages such as the fabrication of novel products, lower energy consumption, and longer durability (Ourimi and Nezhadnaderi 2020). Nanoparticles as nano-adsorbents are frequently reported to have outstanding ability in controlling heavy metal pollution through adsorptive

✉ Wan Norharyati Wan Salleh
hayati@petroleum.utm.my

1 Advanced Membrane Technology Research Centre (AMTEC), Universiti Teknologi Malaysia, 81310 Skudai, Johor, Malaysia

2 School of Chemical and Energy Engineering, Faculty of Engineering, Universiti Teknologi Malaysia, 81310 Skudai, Johor, Malaysia

3 School of Mechanical Engineering, Faculty of Engineering, Universiti Teknologi Malaysia, 81310 Skudai, Johor, Malaysia

4 Department of Civil Engineering, Faculty of Civil Engineering and Built Environment, Universiti Tun Hussein Onn Malaysia, 86400 Parit Raja, Johor, Malaysia

removal due to their high amount of active surface for sorption, excellent porosity, and large specific surface area (Kumari et al. 2019). The high level of flexibility in the treatment of a wide range of toxic wastes is one of the advantages of nano-sorbents in sustaining the environment.

Metal–organic framework (MOF) is known to have tunable pore size and shapes due to the flexibility in the functionalization and metal center and ligand bonding (Pan et al. 2011). One of the most popular MOFs is zeolitic imidazolate framework-8 (ZIF-8), which is made up of zinc salt as the metal center and imidazolate as the ligand surrounding it. ZIF-8 has outstanding advantages in adsorbing heavy metal ions due to its ultrahigh porosity, aside from its ease of synthesis and outstanding thermal and chemical stabilities (Li et al. 2021). There is an extensive study of MOF in various applications such as the adsorption of volatile organic compounds (Zhou et al. 2016), carbon dioxide adsorption (Pokhrel et al. 2018), removal of dyes (Abdi et al. 2017), and heavy metals adsorption (Huang et al. 2018; Li et al. 2014).

By controlling specific parameters during the synthesis process, it has a significant impact on the product properties (Singh et al. 2021). The preparation conditions of ZIF-8 such as the ratio of zinc salt and linkers, type of zinc salt, temperature, and type of solvents have a significant impact on the pore distribution, particle size, and morphology of the particles formed (Jin and Shang 2021). Besides that, Li et al. (2021) also emphasized that the purity of ZIF-8 formed is directly influenced by the content of linkers, the temperature for crystallization, and the type of solvents used. The role of solvent has a direct impact on the coordination of the self-assembly process of ZIF-8, thermodynamically and kinetically. In addition, a solvent can act as guest molecules, ligands, both guest molecules and ligands, or as structure directing agent (SDA) (Li and Du 2011). Solvents in the preparation of ZIF-8 mainly acted as the structure directing agent or a template, which still have a direct influence over the physicochemical properties of ZIF-8. Bustamante et al. (2014) studied the influence of different solvents: aliphatic alcohols, water, and dimethylformamide on the synthesis of ZIF-8, thereby concluding that solvent altered the reaction evolution involving crystallization rate and crystallite size.

On the other hand, in this study, the role of polar protic solvents, such as aqueous solution, methanol, and ammonia solution, was studied for the synthesis of ZIF-8, denoted by ZIF-8 (H), ZIF-8 (M), and ZIF-8 (N), respectively. All ZIF-8s formed were characterized for the functional groups present, crystallinity, crystallite size, and morphology. Besides investigating the characterization of the synthesized ZIF-8, this study will attempt to discover the effects of different solvents on the performance of ZIF-8 adsorbing Pb(II) and Cd(II). Therefore, the exploration of ZIF-8 synthesized using different solvents not only covers the physicochemical properties of the synthesized ZIF-8, but also extended to its direct application as adsorbent. The mechanism of Pb(II) and Cd(II) sorption in terms of isotherms and kinetics was also examined.

Materials and methods

Materials and chemicals

Lead nitrate ($Pb(NO_3)_2$, cadmium nitrate tetrahydrate ($Cd(NO_3)_2{\cdot}4H_2O, > 98\%$), zinc nitrate hexahydrate ($Zn(NO_3)_2{\cdot}6H_2O, > 98\%$), and 2-methylimidazole (Hmim, > 99%) were purchased from Sigma Aldrich. Methanol AR grade, ammonia solution (25%), and triethylamine (TEA, $(C_2H_5)_3\,N, > 99\%$) were bought from Merck. No further purification was done on all the chemicals used prior to the experiments.

Synthesis of ZIF-8

In general, the procedure in the preparation of ZIF-8s was carried out following the room temperature synthesis (RTS) using three different solvents: aqueous solution (ZIF-8 (H), methanol (ZIF-8 (M)), and ammonia solution (ZIF-8 (N)).

The synthesis of ZIF-8 (H) was conducted following the method demonstrated by Khan et al. (2018). In 200 mL of RO water, 2.95 g of zinc nitrate hexahydrate was dissolved. In another beaker containing 200 mL of RO water, 6.5 g of 2-methylimidazole was dissolved and 15 mL of TEA was subsequently added. TEA is a base-type additive, which acted as the deprotonating agent for the formation of ZIF-8. Then, the solution containing zinc salt was poured into the 2-methylimidazole solution under stirring conditions and continuously stirred for 40 min. The mixture was subjected to centrifugation at 10,000 rpm for 10 min. The product to be collected was washed repeatedly using RO water and then dried in the oven overnight.

On the other hand, the preparation of ZIF-8 (M) using methanol as the solvent was adapted from the method demonstrated by Li et al. (2019). Similar to the preparation of ZIF-8 (H), two separate beakers containing solvents were used. In Beaker A, 70 mL of methanol was needed to dissolve 1.5 g of zinc nitrate hexahydrate. In Beaker B, 3.3 g of 2-methylimidazole was added to the beaker containing 70 mL methanol. Then, the zinc solution in Beaker A was poured into Beaker B and the mixture was continuously stirred for 24 h. The product of ZIF-8 (M) was collected by repeated centrifugation at 4000 rpm for 5 min using methanol as the washer and left for drying overnight in an oven at 80 °C.

ZIF-8 (N) was prepared using an aqueous ammonia solution as the solvent (Shams et al. 2016). In 3 mL of RO water, 0.594 g of zinc nitrate hexahydrate was dissolved. On the other

hand, 0.328 g of 2-methylimidazole was dissolved in another beaker containing 3.76 g of ammonium hydroxide solution. After that, the zinc salt solution was rapidly poured into the beaker containing 2-methylimidazole and ammonia solution. Then, the mixture was stirred for 10 min and brought for centrifugation. The centrifugation was done repeatedly at 3000 rpm for 10 min and the product was washed a few times using RO water. ZIF-8 (N) was then collected after oven-drying overnight.

Characterization of adsorbents

ZIF-8 (H), ZIF-8 (M), and ZIF-8 (N) adsorbents were characterized using Fourier-transform Infrared Spectrometer (FT-IR), X-ray Diffraction (XRD), Scanning Electron Microscopy (SEM), and Field-Emission Scanning Electron Microscopy (FE-SEM) analyses. FT-IR analysis was done to identify the functional groups present in the adsorbents. A small amount of adsorbent powder was mixed with potassium bromide (KBr) and pressed to form a KBr pellet. Then, the pellet was analyzed using an FT-IR Perkin Elmer spectrometer and scanned at the wavenumber ranging from 400 to 4000 cm^{-1}. XRD analysis was done for the crystallinity associated analysis and the identification of the adsorbents synthesized. The instrument used was Rigaku Smartlab X-ray Diffractometer using Cu K_α radiation ($\lambda_{XRD}=0.154$ nm) and the XRD patterns were scanned in the range of 3–100°, at 0.02 step width. The morphology of adsorbents was studied using the SEM model Hitachi TM3000 Tabletop Microscope, whereas FE-SEM analysis was conducted by coating the adsorbents with platinum and analyzed using model Hitachi SU8020 with an accelerating voltage of 2000 V.

Adsorption test

The adsorption test of Pb(II) and Cd(II) onto ZIF-8 (H), ZIF-8 (M), and ZIF-8 (N) was generally carried out in 100 mL centrifuge tubes containing 0.01 g of individual adsorbents and 25 mL of Pb(II) or Cd(II) solutions. The mixture was shaken at a constant rate of 250 rpm for 24 h using a platform shaker. The sample after adsorption was collected using 0.45 µm syringe filter and analyzed for the concentration of heavy metals using Flame Atomic Absorption Spectroscopy. The adsorption capacity, q and removal efficiency, were calculated using Eqs. (1) and (2):

$$\text{Adsorption capacity} = \frac{(C_i - C_f)}{m} \times V, \tag{1}$$

$$\text{Removal efficiency} = \frac{(C_i - C_f)}{C_i} \times 100. \tag{2}$$

C_i (mg/L) is the initial concentration of Pb(II) or Cd(II) solution before adsorption, while C_f (mg/L) is the final concentration of the Pb(II) or Cd(II) solution after adsorption. V (L) is the volume of Pb(II) or Cd(II) solution used and m(g) is the mass of the adsorbents. The synthetic solutions were prepared by preparing the 1000 mg/L stock solution of Pb(II) using 1.5895 g of zinc nitrate hexahydrate, and Cd(II) using 2.7442 g of cadmium nitrate tetrahydrate, dissolved using RO water in 1000 mL volumetric flask. Then, the stock solution was diluted to a desired concentration.

The effect of solution pH was investigated using 0.01 g of adsorbents in 50 mL of 100 mg/L Pb(II) and Cd(II) solution. The initial pH of the solution was adjusted to pH 3 until pH 6 for Pb(II) solution, while that of Cd(II) solution were adjusted to pH 3 to 8 using 0.1 M NaOH and 0.1 M HCl solution. On the other hand, the effect of initial concentration was investigated using 25 mL of 20, 40, 60, 80, and 100 mg/L of Pb(II) or Cd(II) solution with 0.01 g of adsorbents. 0.005, 0.01, 0.015, 0.02, and 0.025 g of adsorbents in 25 mL of 100 mg/L heavy metal solutions were used to study the effect of adsorbent dosage. The parameters utilized in investigating the effect of contact time were picked based on the optimum values obtained from the adsorption test. For Pb(II) adsorption, 0.02 g of adsorbents were mixed into 20 mg/L of Pb(II) solution, whereas Cd(II) adsorption was done using 0.025 g of adsorbents in 20 mg/L of Cd(II) solution. An amount of 15 mL of the sample was collected at the designated interval time and filtered prior to AAS analysis. The effect of competing ions was carried out using 25 mL of 10 mg/L competing ions (Fe(II), Zn(II), Cu(II), or Pb(II)/Cd(II)) mixed with 25 mL of 10 mg/L Pb(II) or Cd(II) solution. All tests were done in triplicate and dilution may be needed for samples of high heavy metals concentration, which might interfere with the detection limit of the Atomic Absorption Spectrometry (AAS) instrument.

Results and discussion

Characterization of adsorbents

FT-IR spectra analysis

The FT-IR analysis was done to identify the functional groups present in the adsorbents (Gudimella et al. 2022). The FT-IR spectra are shown in Fig. 1a, which illustrates that all synthesized ZIF-8 s obtained similar spectra. All spectra of the prepared ZIF-8 s showed a band approximately at 3419 cm^{-1} corresponding to the stretching of the N–H bond, whereas a band at 2926 cm^{-1} presented the C–H vibrational modes for methyl groups in the linker (Kaur et al. 2017). Apart from that, the peak observed at 1567 cm^{-1} was related to the C=C stretching of the cyclic alkene of the

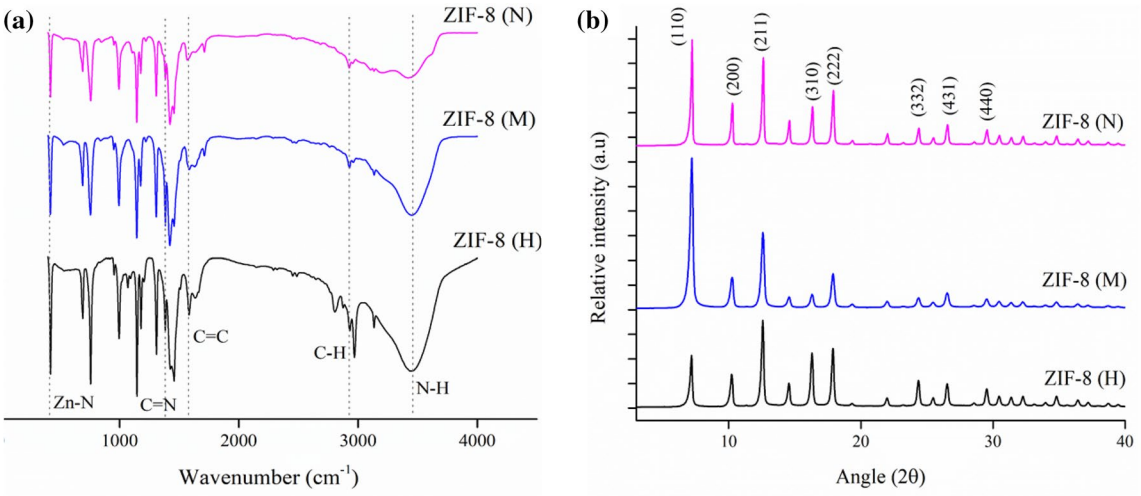

Fig. 1 **a** FT-IR spectra and **b** XRD patterns for ZIF-8 (N), ZIF-8 (M), and ZIF-8 (H) adsorbents

imidazolate. The peak present at 1423 cm^{-1} corresponded to the stretching bond of C=N found on the linker as similarly reported by Binaeian et al. (2020). Meanwhile, the presence of a strong peak found at 421 cm^{-1} was attributed to the Zn-N bond originating from the connection between the Zn atom at the center and the N atom from the imidazolate linker (Arabkhani et al. 2021). Various peaks found between 1308 and 995 cm^{-1} were related to the in-plane bending of the ring, while the peak found at 759 cm^{-1} referred to the out-of-plane bending of the ring (Abdi et al. 2017).

XRD analysis

XRD patterns of all the synthesized ZIF-8 s were exhibited in Fig. 1b, which confirmed that all solvents were successful in producing ZIF-8s with high crystallinity, as demonstrated by the sharp XRD patterns generated by the materials with the ordered arrangement (Hou et al. 2014). The patterns were in good agreement with the phase name in the library; ZIF-8, activated, Basolite Z1200T (DB card number: 00-062-1030). Similar findings were also reported from previous studies (Thomas et al. 2016; Zhang et al. 2018). Characteristic peaks for ZIF-8 were found at 2θ = 7.2°, 10.3°, 12.6°, 16.4°, 17.9°, and 24.4° assigned sequentially to the diffraction of (110), (200), (211), (310), (222), and (332) planes. Besides that, the crystallinity index (CI) for all materials was determined following the method reported by Khan et al. (2019) and Navarro-pardo et al. (2013), as shown in Eq. 3:

$$CI = \frac{A_c}{A_c + A_a}, \tag{3}$$

where A_c is the integrated area for the crystalline peaks, and A_a is the integrated area for the amorphous halo. The integrated areas were determined using peak-fitting of Gaussian functions in Origin® by decomposing the diffraction pattern. The CI of ZIF-8 (N), ZIF-8 (M), and ZIF-8 (H) were 85.97%, 91.63%, and 90.01%, respectively, which reflected that all ZIF-8s synthesized have a high degree of crystallinity. Thus, all solvents were capable of synthesizing highly crystalline ZIF-8s, with the least CI obtained by ZIF-8 (N).

Morphological properties of adsorbents

The surface morphology of the adsorbents was analyzed using SEM analysis, and the images captured are shown in Figs. 2a–c. At the magnification of x10k, only ZIF-8 (N) showed a clear image of cubic shapes which were distributed over a wide area, while ZIF-8 (H) and ZIF-8 (M) did not show a distinct shape. Nevertheless, from the SEM image, it could be seen that ZIF-8 (H) was spread more evenly, as compared to ZIF-8 (M) which showed a sign of agglomeration. The dissimilar ability of different solvents in particle dispersion, thus, resulted in different levels of aggregation, in which methanol showed a greater tendency in forming agglomerated particles, as compared with aqueous solution and ammonia solution (Bustamante et al. 2014).

Since SEM analysis utilized has a limitation in providing a clearer image, the morphology of all adsorbents was further analyzed using FE-SEM analysis as illustrated in Figs. 2d–i. ZIF-8 (N) showed a significantly greater particle size, as compared with ZIF-8 (H) and ZIF-8 (M). The average particle size of ZIF-8 (N) was 573 nm, whereas ZIF-8 (H) and ZIF-8 (M) had average sizes of 108 nm and 62 nm, respectively. The morphology of ZIF-8 (N) resembled the cube with truncated edges, similarly discussed by Troyano et al. (2019), with the {100} plane as the six faces of the

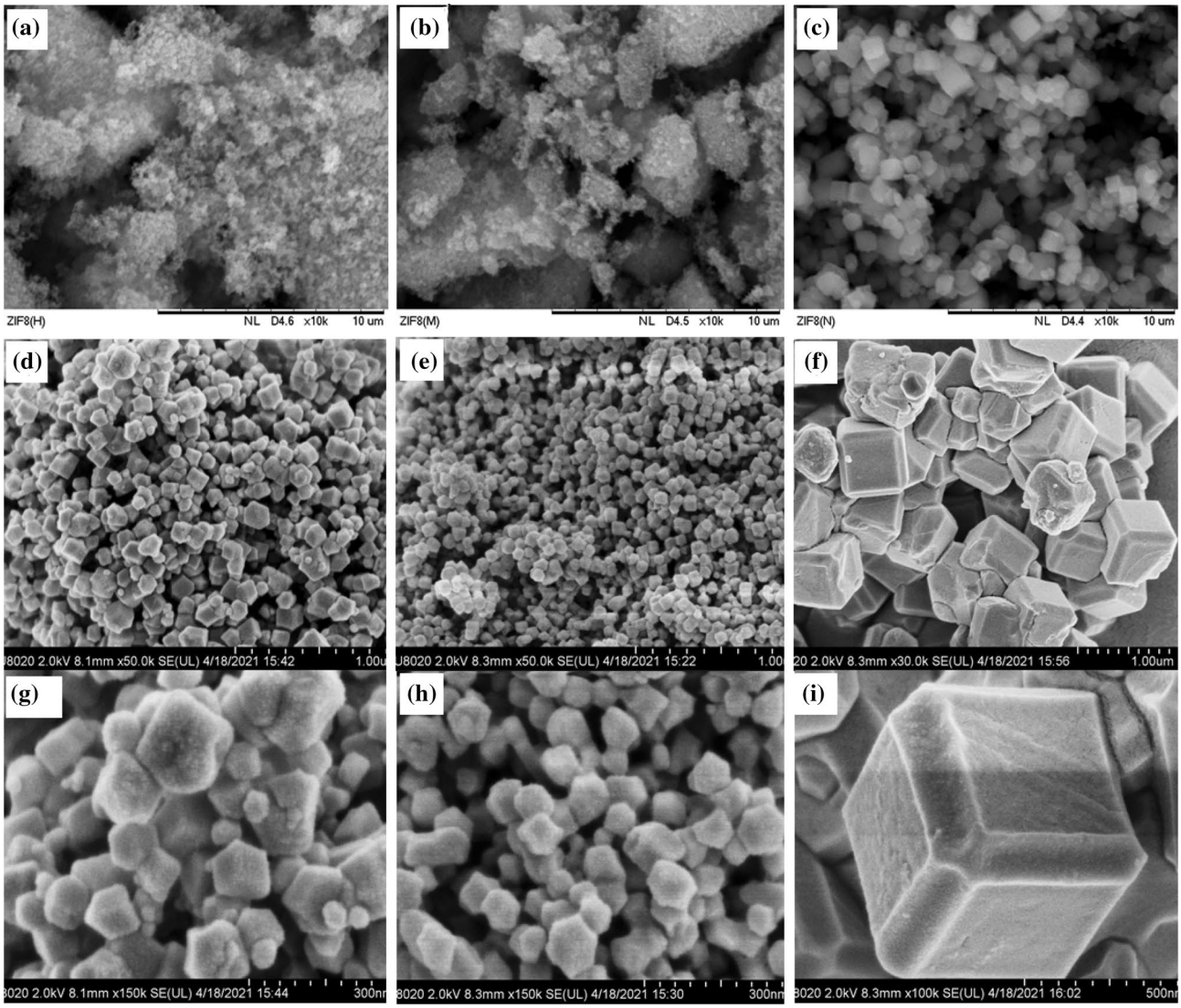

Fig. 2 Images for SEM analysis of **a** ZIF-8 (H) at ×10k, **b** ZIF-8 (M) at ×10k, **c** ZIF-8 (N) at ×10k, and FE-SEM analysis of **d** ZIF-8 (H) at×50.0 k, **e** ZIF-8 (M) at×50.0 k, **f** ZIF-8 (N) at×30.0 k, **g** ZIF-8 (H) at x150k, **h** ZIF-8 (M) at x150k, and **i** ZIF-8 (N) at ×100k

cubes, while the {110} plane is the truncated edge. As mentioned by Schejn et al. (2014), the evolution of crystal morphology with time started with cube, followed by a cube with truncated edges, a rhombic dodecahedron with truncated edges, and lastly the most complete crystal, a rhombic dodecahedron. ZIF-8 (N) showed an intermediate stage of crystal morphology, while ZIF-8 (M) showed a complete crystal morphology of rhombic dodecahedrons. The use of free-additive methanol has been reported to produce a rhombic dodecahedral ZIF-8 from the simpler species grown to the more stabilized form (Moh et al. 2013). On the other hand, ZIF-8 (H) demonstrated a mixture of two phases: cubic shape and the rhombic dodecahedron with truncated corners (Jian et al. 2015). The rhombic dodecahedron with truncated corners occurred where the {110} facet became more visible, as compared with the plane of the cube with the truncated edge. The surface energy of the crystal facet has a significant impact on the determination of morphology. Therefore, the rhombic dodecahedron has lower energy, making it more stable, as compared with the cubic shape (Malekmohammadi et al. 2019). Thus, in this study, methanol as the solvent synthesized a complete morphology of ZIF-8 crystal, whereas ZIF-8 (H) and ZIF-8 (N) produced an intermediate ZIF-8s phase.

In addition, the EDX mapping for ZIF-8 (H), ZIF-8 (M), and ZIF-8 (N) are illustrated in Fig. 3. The distribution of elements of C, Zn, N, and O is homogenously scattered for all ZIF-8 synthesized. By looking at the weight percentage of the elements, C is found to be the most dominant followed by N, Zn, and O. ZIF-8 (H) showed the greatest amount of

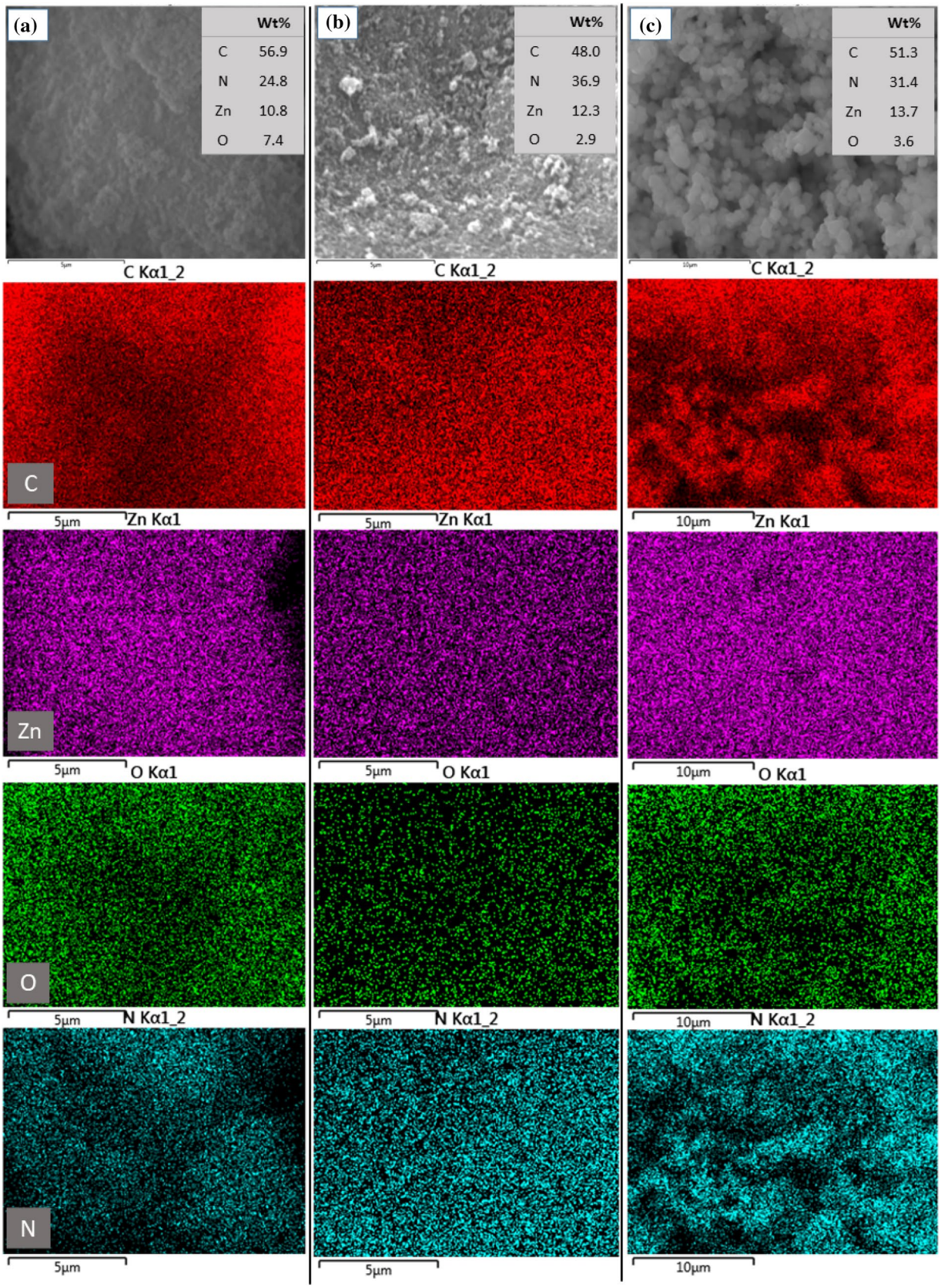

Fig. 3 EDX mapping of C, Zn, O, and N for **a** ZIF-8 (H), **b** ZIF-8 (M), and **c** ZIF-8 (N) adsorbents

O (7.4%), as compared with 3.9% for ZIF-8 (N), and the least was 2.9% for ZIF-8 (M), which could be a significant factor for the superior performance of ZIF-8 (H) and ZIF-8 (M) in adsorbing Pb(II) and Cd(II), as compared to ZIF-8 (M). The oxygen-containing compounds were well known to notably involved in the adsorption by providing the sites for electrostatic attraction and complexation of the heavy metals (Liao et al. 2021).

Adsorption study of Pb(II) and Cd(II)

Effects of initial pH solution

All as-synthesized ZIF-8s were investigated for their performance in adsorbing Pb(II) and Cd(II) from the synthetic aqueous solution prepared. The initial pH of the solution plays a crucial role in determining the adsorption performance of Pb(II) and Cd(II). Figure 4 shows the effects of initial pH and initial concentration on the performance of ZIF-8 (H), ZIF-8 (M), and ZIF-8 (N) in removing Pb(II) and Cd(II) in terms of adsorption capacity and removal efficiency. For Pb(II) adsorption, the increase in pH generally caused an increase in the adsorption performance. At pH 6, the Pb(II) adsorption capacity of ZIF-8 (M), ZIF-8 (H), and ZIF-8 (N) was reported at 395.02 mg/g, 401.00 mg/g, and 475.54 mg/g, respectively. ZIF-8 (N) showed the greatest removal efficiency, and successfully removed 95% of Pb(II) at pH 6. At pH greater than 6, lead hydroxides started to precipitate out, thus interfering with the adsorption of Pb(II) and causing the removal following the precipitation mechanism instead of adsorption.

Meanwhile, Cd(II) removal showed an increasing trend for the increase in pH until reaching the optimum pH of 7, then decreased at the initial solution of pH 8. At pH 7, ZIF-8 (H) demonstrated the greatest Cd(II) adsorption capacity of 339.55 mg/g with removal efficiency of 75.46%, followed by ZIF-8 (M) with 276.65 mg/g (50.41%), and ZIF-8 (N) with 209.80 mg/g (38.23%). At acidic pH, both Pb(II) and Cd(II) competed with an excessive amount of proton for the adsorption site on the surface of adsorbents. Therefore, the removal performance of positively charged Pb(II) and Cd(II) at acidic pH was less favorable (Ahmad et al. 2021). Meanwhile, as the pH increased reached the neutral pH, the amount of proton was relatively lower, thus adsorption of Pb(II) and Cd(II) showed a positive increment until they reached the

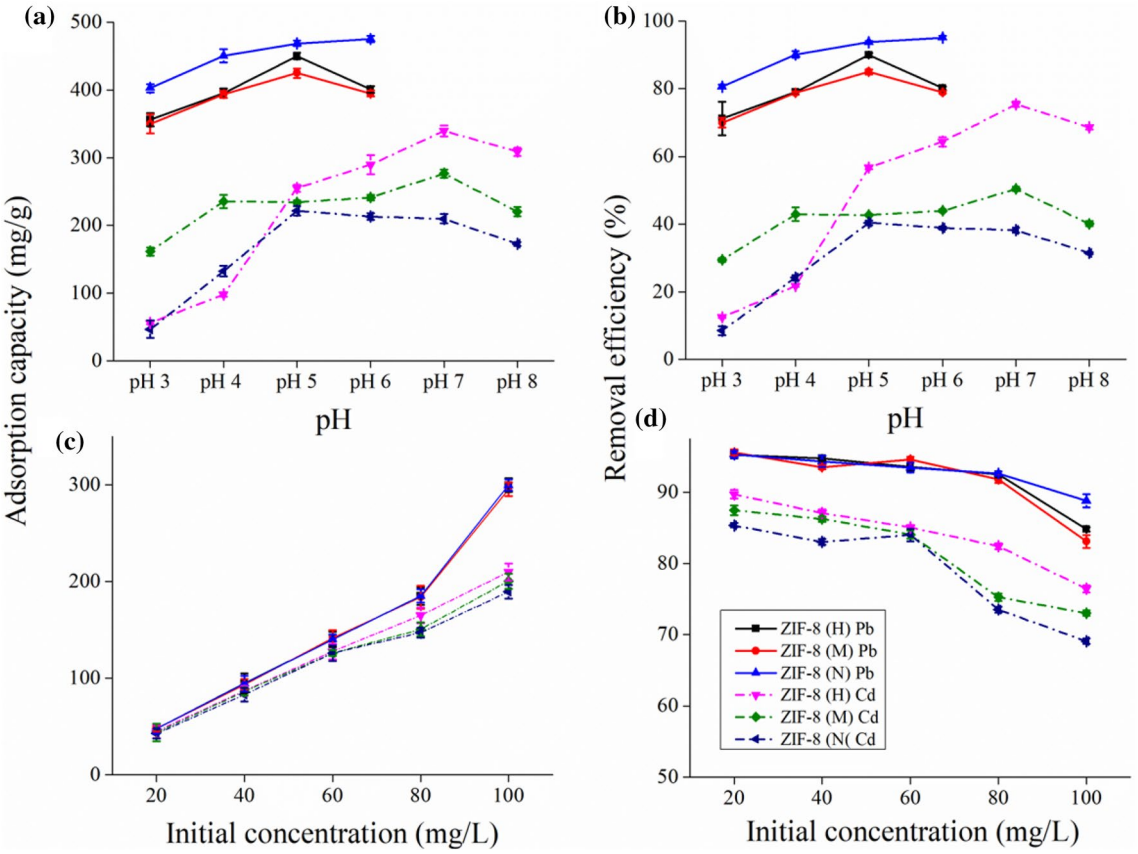

Fig. 4 Adsorption test of Pb(II) and Cd(II) of the effects of initial pH on the **a** adsorption capacity and **b** removal efficiency, and the effects of initial concentration on the **c** adsorption capacity and **d** removal efficiency

optimum pH. As the pH increased to the more basic condition, OH^- interfered with the adsorption performance (Ahmad et al. 2020a). The isoelectric points (IEP) for ZIF-8 (H), ZIF-8 (M), and ZIF-8(N) were determined to be at pH less than 2, 2.76, and 3.04, respectively. These values showed that the adsorbents were positively charged at a pH lower than IEP, which inhibits the adsorption of the positively charged Pb(II) and Cd(II). On another note, at pH values greater than IEP, the adsorbents were negatively charged, which gradually favored the adsorption of the Pb(II) and Cd(II) which have the opposite charges (Zhu et al. 2015). In a nutshell, the adsorption of Pb(II) and Cd(II) at a greater pH rather than at a very acidic is feasible when using ZIF-8 (H), ZIF-8 (M), and ZIF-8 (N).

Effects of initial concentration

Figure 4c, d illustrates the effects of initial concentration on the adsorption capacity and removal efficiency of Pb(II) and Cd(II) ions. In general, Pb(II) obtained a greater removal performance as compared with Cd(II). This might be due to the smaller hydrated ionic radius of Pb^{2+} over Cd^{2+} ions, of 0.401 nm and 0.426 nm, respectively, as well as the lower hydration energy of Pb^{2+} ((− 1481 kJ/mol) compared to Cd^{2+} ((− 1807 kJ/mol) (Mobasherpour et al. 2012). In addition, the adsorption capacity increased with the increase of initial concentration. ZIF-8 (H), ZIF-8 (M), and ZIF-8 (N) obtained similar Pb(II) adsorption capacities while for Cd(II) adsorption, ZIF-8 (H) showed slightly greater performance, followed by ZIF-8 (M) and ZIF-8 (N). At the initial concentration of 100 mg/L, ZIF-8 (H), ZIF-8 (M), and ZIF-8 (N) had Pb(II) adsorption capacity of approximately 299 mg/g for all adsorbents, while for Cd(II), the adsorption capacities reached 209.79 mg/g, 200.41 mg/g, and 189.53 mg/g, respectively. All ZIF-8s managed to remove up to 95% of 20 mg/L Pb(II) while ZIF-8 (H) obtained the removal efficiencies of 89.69% while removing 20 mg/L Cd(II), followed by ZIF-8 (M) with 87.45%, and ZIF-8 (N) with 85.33%. The highest adsorption capacity was obtained using 100 mg/L Pb(II) and Cd(II), although the removal efficiency was lower than that of 20 to 60 mg/L initial concentration. This phenomenon might be related to the decrease in the available adsorption sites due to the saturated sites occupied by the greater amount of Pb(II) and Cd(II) adsorbed at 100 mg/L initial concentration (Moharram et al. 2016). Therefore, considering the highest removal efficiency of Pb(II) and Cd(II) obtained (> 85%), the optimum initial concentration for Pb(II) and Cd(II) adsorption was chosen at 20 mg/L and used for the initial concentration on the investigation of the contact time.

Effects of adsorbent dosage

The effects of adsorbent dosage were studied in the range of 5–25 mg/L of adsorbents to remove 100 mg/L of Pb(II or Cd(II) solutions. For Pb(II) adsorption, all adsorbents showed a consistent trend in the adsorption capacities and the removal efficiencies until they reached the highest point at 323.60 mg/g (95.85%) for ZIF-8 (N), followed by 310.44 mg/g (91.50%) for ZIF-8 (H), and 310.76 mg/g (92.04%) for ZIF-8 (M) while using 20 mg dose of adsorbents. Meanwhile, a 25 mg dose of adsorbents caused a decrease in both adsorption capacities and removal efficiency. This could be attributed to the aggregation of a high amount of adsorbents, thus leading to a decrease in total active sites exposed for adsorption (Alghamdi et al. 2019). On another note, the adsorption of Cd(II) showed a gradual decrease to the steady adsorption capacities with the increase in the adsorbent dosage. This was followed by a gradual increase in stable removal efficiencies of Cd(II), which were especially apparent for ZIF-8 (H) and ZIF-8 (N). The decrease in the adsorption capacity could be due to the increase in the number of available sites for adsorption or the agglomeration of adsorbents, which might lead to a longer diffusion pathway (Mosoarca et al. 2020). By comparing the greatest removal efficiency for both Pb(II) and Cd(II) removal with respect to the adequate adsorption capacity, 20 mg doses of ZIF-8 (H), ZIF-8 (M), and ZIF-8 (N) are the optimum doses to be used.

Effects of contact time

Figure 5c, d illustrates the effects of contact time on the adsorption of Pb(II) and Cd(II) by reporting the adsorption capacity and removal efficiency using ZIF-8 (H), ZIF-8 (M), and ZIF-8 (N) as adsorbents. For both Pb(II) and Cd(II) adsorption, ZIF-8 (N) successfully removed up to 98% of Pb(II) and Cd(II) within the first 15 min. Meanwhile, both ZIF-8 (H) and ZIF-8 (N) removed 98% Pb(II) within 240 min, while 300 min was needed to remove 99% Cd(II). Thus, the optimum contact time for Pb(II) and Cd (II) adsorption varies with the different solvents used in which, ZIF-8 (N) needed only 15 min, ZIF-8 (M) and ZIF-8 (N) needed 240 min and 300 min for Pb(II) and Cd(II) adsorption, respectively. ZIF-8 (N) adsorbed Pb(II) and Cd(II) in two stages: rapid sorption and near equilibrium process, while ZIF-8(H) and ZIF-8 (M) involved three stages of adsorption: rapid sorption, slow sorption, and near equilibrium process (Ahmad et al. 2020b). ZIF-8 (N) may have a clearer adsorption pathway for an adequate amount of adsorption site, which leads to rapid sorption for reaching equilibrium. Slower adsorption occurred on the surface of ZIF-8 (M) could be associated with the tendency of ZIF-8 (M) to aggregate as depicted in the previous SEM image in

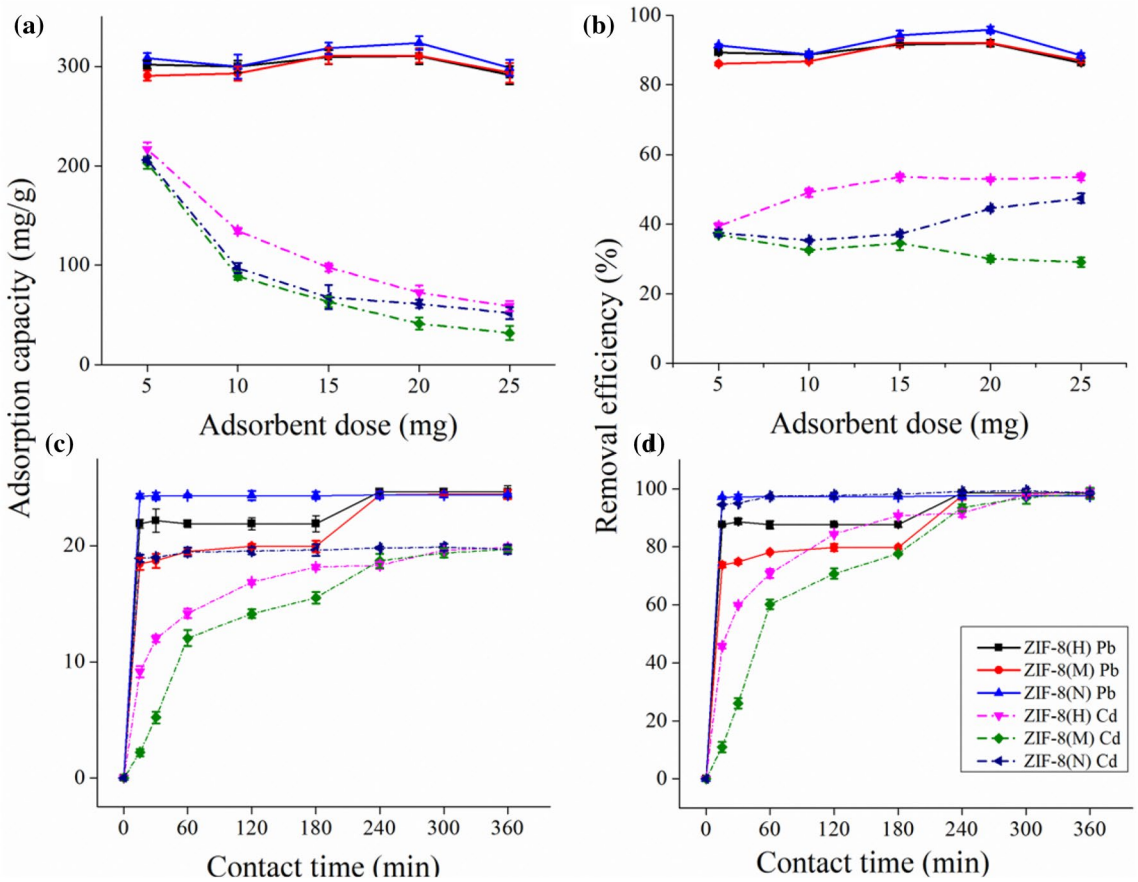

Fig. 5 Adsorption test of Pb(II) and Cd(II) of the effects of adsorbent dosage on the **a** adsorption capacity and **b** removal efficiency, and the effects of contact time on the **c** adsorption capacity and **d** removal efficiency

Fig. 2. The agglomeration of adsorbents, thus, resulted in the reduction of available surface for adsorption. The difference in adsorption capacity is related to the difference in the optimum adsorbent dosage applied, where 1.0 g/L and 0.8 g/L adsorbents were used to remove 20 mg/L of Pb(II) and Cd(II) solution, respectively.

Effects of competing ions

In actual wastewater, competing ions such as Fe(II), Zn(II), and Cu(II) can be found, with possible interference of equally positively charged ions that might interfere with the performance of the adsorption. Therefore, it is essential to investigate the effects of competing ions and the selectivity of ZIF-8s adsorbents towards Pb(II) and Cd(II). In Fig. 6, it can be observed that the adsorption of Pb(II) was not significantly affected by the existence of competing ions. Meanwhile, the adsorption of Cd(II) using ZIF-8 (H) was positively influenced by the presence of competing ions, achieving 100% removal. On the contrary, competing ions have negative impacts on the Cd(II) adsorption using ZIF-8 (M) and ZIF-8 (N). ZIF-8(N) obtained 75.84%, 75.15%, 68.98%, and 70.29% removal percentage of Cd(II), while ZIF-8 (M) obtained 67.23%, 75.53%, 73.42%, and 86.11% with the presence of Fe, Zn, Cu, and Pb in the solution, respectively. The competition between adsorption might be primarily governed by the hydration energy, where Pb(II) and Cd(II) have relatively lower energy as compared with Fe(II), Zn(II), and Cu(II) ions (Panayotova and Velikov 2003). Considering the effects of competing ions on both Pb(II) and Cd(II) adsorption, ZIF-8 (H) is more likely to produce an outstanding performance when used in actual wastewater.

Adsorption isotherms and kinetics

Langmuir and Freundlich isotherms

The insight on the mechanism of Pb(II) and Cd(II) adsorption and the possible interaction between the adsorbents and heavy metal solutions could be investigated by plotting the adsorption isotherm possible. The equations for the Langmuir and Freundlich isotherm are expressed as in Eqs. 4 and 5, respectively:

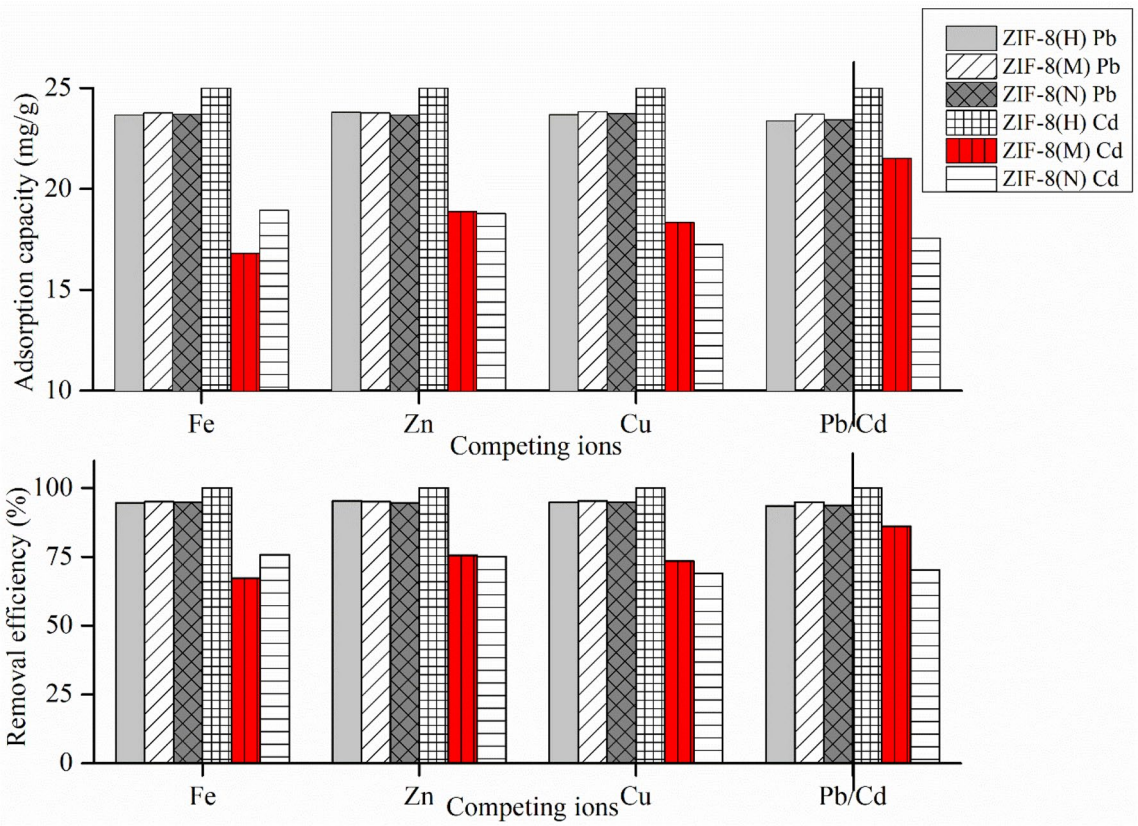

Fig. 6 The effects of competing ions on the adsorption capacities and removal efficiencies of Pb(II) and Cd(II) adsorption

$$\frac{C_e}{q_e} = \frac{1}{q_m} C_e + \frac{1}{K_L q_m}, \tag{4}$$

$$\log q_e = \log K_f + \frac{1}{n} \log C_e, \tag{5}$$

where C_e (mg/L) is the concentration of Pb(II) or Cd(II) in equilibrium, q_e (mg/g) is the adsorption capacity of Pb(II) or Cd(II) in equilibrium, while q_m (mg/g) is the maximum adsorption capacity for Langmuir isotherm. K_L and K_f are the Langmuir constant related to the binding site affinity and the Freundlich constant related to intensity, respectively. Meanwhile, n represents the heterogeneity coefficient of the Freundlich isotherm. The Langmuir plot of C_e/q_e against Ce revealed the maximum adsorption capacity of the adsorbents, as calculated from the reciprocal of the gradient of the plot. Meanwhile, Freundlich isotherm involved the graph of $log\ q_e$ versus $log\ C_e$, in which the intercept and the gradient could be used to calculate K_f and n, respectively. Table 1 summarizes the parameters and correlation coefficients obtained from the plot of Langmuir and Freundlich isotherms, as well as the pseudo-first-order and pseudo-second-order kinetic models. The values of correlation coefficients (R^2) obtained by the Langmuir isotherm for all adsorbents were nearer to 1, as compared with the Freundlich isotherm, which was also obtained by previous studies (Gabris et al. 2018; Shahzad et al. 2017). Thus, this inferred that Langmuir isotherm was the more appropriate model for describing the Pb(II) and Cd(II) adsorption using ZIF-8 (H), ZIF-8 (M), and ZIF-8 (N). Thus, as represented by Langmuir isotherm, the adsorption of Pb(II) and Cd(II) on the surface of ZIF-8 s occurred through monolayer sorption, where adsorption occurred in uniformity and through homogeneous binding sites (Ali 2018).

Adsorption kinetics

The equations of the pseudo-first-order and the pseudo-second-order are described in Eqs. (6) and (7), respectively:

$$\ln\left(q_e - q_t\right) = \ln q_e - k_1 t, \tag{6}$$

$$\frac{t}{q_t} = \frac{1}{k_2 q_e^2} + \frac{1}{q_e} t. \tag{7}$$

q_t is the adsorption capacity of Pb(II) or Cd(II) at the respected time, t, while k_1 and k_2 are the rate constants for the pseudo-first-order and the pseudo-second-order

Table 1 Parameters and correlation coefficients for adsorption isotherms and kinetics of Pb(II) and Cd(II) adsorption using ZIF-8 (H), ZIF-8 (M), and ZIF-8 (N)

Isotherm/Kinetic	Parameter		ZIF-8 (H)	ZIF-8 (M)	ZIF-8 (N)
Langmuir	q_{max} (mg/g)	Pb(II)	454.55	434.78	476.19
		Cd(II)	312.50	277.78	263.16
	K_L (L/mg)	Pb(II)	0.1189	0.1264	0.1105
		Cd(II)	0.0777	0.0774	0.0712
	R^2	Pb(II)	0.9947	0.9691	0.9949
		Cd(II)	0.9980	0.9632	0.9660
Freundlich	K_f	Pb(II)	54.2251	55.8048	53.2476
		Cd(II)	30.4089	28.9201	26.0976
	n	Pb(II)	1.7342	1.7467	1.7263
		Cd(II)	1.6098	1.7153	1.7062
	R^2	Pb(II)	0.9861	0.9684	0.9904
		Cd(II)	0.9865	0.9575	0.9320
Pseudo-first-order	K_1 (1/min)	Pb(II)	0.0226	0.0210	0.0010
		Cd(II)	0.0123	0.0129	0.0241
	q_e (mg/g)	Pb(II)	12.7101	21.2793	0.2462
		Cd(II)	14.2321	21.8872	2.6269
	R^2	Pb(II)	0.7737	0.8088	0.0032
		Cd(II)	0.9303	0.9518	0.6811
Pseudo-second-order	K_2 (g/mg.min)	Pb(II)	3.7563	0.0016	0.2668
		Cd(II)	1.86×10^{-3}	0.29×10^{-3}	45.12×10^{-3}
	q_e (mg/g)	Pb(II)	1.0038	24.8139	24.3902
		Cd(II)	21.0084	27.3224	19.8413
	R^2	Pb(II)	0.9962	0.9881	1.000
		Cd(II)	0.9982	0.9558	0.9999

kinetic models, respectively (Shanmugaraj et al. 2022). The plot of $ln(q_e\text{-}q_t)$ against t indicated the pseudo-first-order kinetics, where the slope of the graph represents the rate constant. On the other hand, the rate constant for the pseudo-second-order model could be obtained from the intercept of the graph of t/q_t versus t. According to Table 1, the values of R^2 obtained by all adsorbents while plotting the pseudo-second-order kinetic model for both Pb(II) and Cd(II) adsorption are closer to 1, as compared with the pseudo-first-order kinetic model, frequently reported by previous studies (Janusz et al. 2022; Shirivastava 2015). This suggests that the adsorption of Pb(II) and Cd(II) on the surface of ZIF-8 (H), ZIF-8 (M), and ZIF-8 (N) had transpired following the chemisorption instead of physisorption (Ge and Ma 2015). Chemisorption involved the formation of chemical bonding which happens via the transfer of electrons either by sharing or electron exchange (Hu et al. 2016). In addition, the concentration of heavy metal ions and the adsorption sites density might play a major role in the adsorption process of Pb(II) and Cd(II on the surface of ZIF-8 (H), ZIF-8 (M), and ZIF-8 (N) (Song et al. 2019).

Adsorption mechanism

The mechanism for the adsorption of Pb(II) and Cd(II) using the synthesized ZIF-8 was evaluated based on the adsorption kinetics and isotherms with the evidence captured by the VPSEM-EDX analysis performed on the adsorbents after adsorption. Figure 7 shows the SEM images of ZIF-8 (H), ZIF-8 (M), and ZIF-8 (N) after the adsorption of Pb(II) and Cd(II). There were significant changes in the morphology of ZIF-8 after the adsorption of Pb(II) and Cd(II). ZIF-8 (H) clearly showed an abundance of particles deposited on its surface, while ZIF-8 (M) showed a greater tendency to agglomerate and form bigger particles compared to the before adsorption. These might be attributed to the interaction between ZIF-8 and heavy metal ions through the electrostatic attraction which could be formed on the surface of ZIF-8. The evidence of the electrostatic attraction could be found in the increase in the weight percentage of oxygen which could be clearly seen in all the synthesized ZIF-8 adsorbents (Nasir et al. 2018). The agglomerated particles might cause a decrease in the available surface sites which reflected why ZIF-8

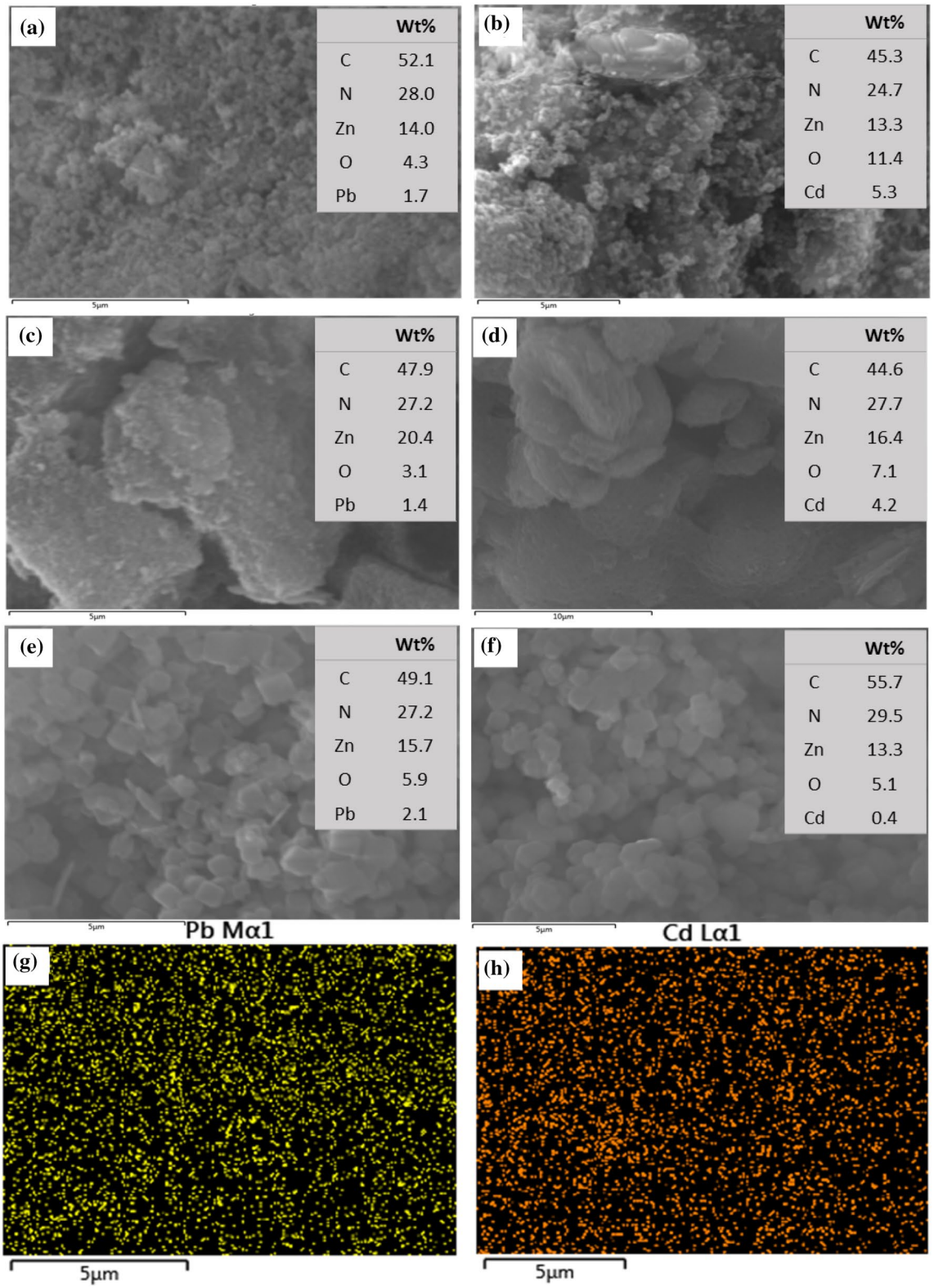

Fig. 7 SEM images and weight percentages of elements obtained by the EDX mapping for **a** ZIF-8 (H) after Pb(II) adsorption, **b** ZIF-8 (H) after Cd(II) adsorption, **c** ZIF-8 (M) after Pb(II) adsorption, **d** ZIF-8 (M) after Cd(II) adsorption, **e** ZIF-8 (N) after Pb(II) adsorption, **f** ZIF-8 (N) after Cd(II) adsorption, **g** EDX mapping of Pb(II) = after adsorption, and **h** EDX mapping of Cd(II) after adsorption

(N) showed the fastest contact time required to adsorb Pb(II) and Cd(II) followed by ZIF-8(H) and ZIF-8(M). Besides that, the EDX mapping showed that Pb(II) and Cd(II) could be found scattered homogeneously on the surface of synthesized ZIF-8 after the adsorption. This corresponded well with the Langmuir isotherm deduction on the adsorption of Pb(II) and Cd(II) that occurred through the monolayer.

Conclusion

In this study, the preparation of ZIF-8 using room temperature synthesis by utilizing different solvents: RO water (ZIF-8 (H)), methanol (ZIF-8 (M)), and ammonia solution (ZIF-8 (N) have successfully synthesized ZIF-8s with high crystallinity, various sizes, and different morphologies. ZIF-8 (H) structure occurred as the mixture of cubic and the rhombic dodecahedrons with truncated edges, while ZIF-8 (N) had the shape of a cube with truncated edges, and ZIF-8 (M) had the most stable crystal shape of the rhombic dodecahedron. The average size of ZIF-8 (N) particles was 573 nm, while ZIF-8 (H) and ZIF-8 (M) had average sizes of 108 nm and 62 nm, respectively. All ZIF-8 s showed good affinity towards the Pb(II) and Cd(II) adsorption. ZIF-8(N) demonstrated the best performance in removing Pb(II) while Cd(II) adsorption was conquered by ZIF-8(H). Both Pb(II) and Cd(II) adsorption equilibrium was achieved in 15 min with ZIF-8 (N), while adsorption using ZIF-8 (H) and ZIF-8 (M) reached equilibrium within 240 min and 300 min, respectively. The adsorption of Pb(II) and Cd(II) followed the Langmuir isotherm and pseudo-second-order. The maximum adsorption capacities for Pb(II) and Cd(II) were 454.54 and 312.50 mg/g (ZIF-8 (H)), 434.78 and 277.78 mg/g (ZIF-8 (M)), and 476.19 and 263.16 mg/g (ZIF-8 (N)), respectively. ZIF-8s prepared using three different solvents showed a promising performance to be used as adsorbents for heavy metal ions.

Funding The authors would like to acknowledge the financial support of the Ministry of Higher Education and Universiti Teknologi Malaysia for the financial support provided under Fundamental Research Grant Scheme (FRGS/1/2020/STG05/UTM/02/1, VOT NO. 5F369) and UTM High Impact Research Grant (Project Number: Q.J130000.2451.08G36) in completing this work. S. Z. N. Ahmad would like to acknowledge the support from Universiti Teknologi Malaysia for the ZAMALAH scholarship.

Declarations

Conflict of interest On behalf of all authors, the corresponding author states that there is no conflict of interest.

References

Abdi J, Vossoughi M, Mohammad N (2017) Synthesis of metal-organic framework hybrid nanocomposites based on GO and CNT with high adsorption capacity for dye removal. Chem Eng J 326:1145–1158

Ahmad SZN, Al-Gheethi A, Hamdan R, Othman N (2020a) Efficiencies and mechanisms of steel slag with ferric oxides for removing phosphate from wastewater using a column filter system. Environ Sci Pollut Res 27:35184–35194. https://doi.org/10.1007/s11356-020-09582-7

Ahmad SZN, Salleh WNW, Yusof N, Mohd Yusop MZ, Hamdan R, Awang NA, Ismail AF (2020b) Pb(II) removal and its adsorption from aqueous solution using zinc oxide/graphene oxide composite. Chem Eng Commun. https://doi.org/10.1080/00986445.2020.1715957

Ahmad SZN, Salleh WNW, Ismail NH, Razali NAM, Hamdan R, Ismail AF (2021) Effects of operating parameters on cadmium removal for wastewater treatment using zeolitic imidazolate framework-L/graphene oxide composite. J Environ Chem Eng 9(5):106139. https://doi.org/10.1016/j.jece.2021.106139

Ahmed MA, Samiha TB, Fatma MA, El-Dek SI (2017) Effective Pb2+ removal from water using nanozerovalent iron stored 10 months. Appl Nanosci 7:407–416. https://doi.org/10.1007/s13204-017-0581-z

Alghamdi AA, Saeed WS, Al-kahtani A, Alharthi FA, Aouak T (2019) Efficient adsorption of lead(II) from aqueous phase solutions using polypyrrole-based activated carbon. Materials 12(12):2020

Ali MEA (2018) Synthesis and adsorption properties of chitosan-CDTA-GO nanocomposite for removal of hexavalent chromium from aqueous solutions. Arab J Chem 11(7):1107–1116

Arabkhani P, Javadian H, Asfaram A, Ateia M (2021) Decorating graphene oxide with zeolitic imidazolate framework (ZIF-8) and pseudo-boehmite offers ultra-high adsorption capacity of diclofenac in hospital effluents. Chemosphere 271:129610. https://doi.org/10.1016/j.chemosphere.2021.129610

Awang NA, Norharyati W, Salleh W (2019) Adsorption of cesium from aqueous solution using chitosan beads. Jurnal Teknologi 81(2):135–140

Awes H, Zaki Z, Abbas S, Dessoukii H, Zaher A, Moaty SAA (2021) Removal of Cu2+ metal ions from water using Mg-Fe layered double hydroxide and Mg-Fe LDH/5-(3-nitrophenyllazo)-6-aminouracil nanocomposite nanocomposite for enhancing adsorption properties. Environ Sci Pollut Res 28:47651–47667

Bezzina JP, Ruder LR, Dawson R, Ogden MD (2019) Ion exchange removal of Cu(II), Fe(II), Pb(II)and Zn(II)from acid extracted sewage sludge – resin screening in weak acid media. Water Res 158:257–267. https://doi.org/10.1016/j.watres.2019.04.042

Binaeian E, Maleki S, Motaghedi N, Arjmandi M (2020) Study on the performance of Cd2+ sorption using dimethylethylenediamine-modified zinc-based MOF (ZIF-8-mmen): optimization of the process by RSM technique. Sep Sci Technol (philadelphia) 55(15):2713–2728. https://doi.org/10.1080/01496395.2019.1655056

Bustamante EL, Fernández JL, Zamaro JM (2014) Influence of the solvent in the synthesis of zeolitic imidazolate framework-8 (ZIF-8) nanocrystals at room temperature. J Colloid Interface Sci 424:37–43. https://doi.org/10.1016/j.jcis.2014.03.014

Farouz M, El-Dek SI, Elfaham MM, Eldemerdash U (2022) Eco-friendly sustainable synthetized nano-composite for removal of heavy metals from aquatic environment. Appl Nanosci 12(5):1585–1600. https://doi.org/10.1007/s13204-021-02331-3

Gabris MA, Jume BH, Rezaali M, Shahabuddin S (2018) Novel magnetic graphene oxide functionalized cyanopropyl nanocomposite as an adsorbent for the removal of Pb(II) ions from aqueous

media: equilibrium and kinetic studies. Environ Sci Pollut Res 25:27122–27132
Ge H, Ma Z (2015) Microwave preparation of triethylenetetramine modified graphene oxide/chitosan composite for adsorption of Cr(VI). Carbohyd Polym 131:280–287
Gudimella K, Gedda G, Kumar PS, Babu BK, Yamajala B, Venkateswara B, Kumar D (2022) Novel synthesis of fluorescent carbon dots from bio-based Carica Papaya leaves: optical and structural properties with antioxidant and anti-inflammatory activities. Environ Res 204:111854. https://doi.org/10.1016/j.envres.2021.111854
Hernández P, Santiago-Cuevas A, Palacios-Cabrera C, Thangarasu P, Narayanan J, Kaur H, Singh J, Kumar D, Huerta-Aguilar CA, Singh PP, Vo DV (2022) Development and applications of Ru and Ce based iron oxides as photocatalysts. Mater Lett 313:131720
Hou C, Zhao G, Ji Y, Niu Z, Wang D, Li Y (2014) Hydroformylation of alkenes over rhodium supported on the metal-organic framework ZIF-8. Nano Res 7(9):1364–1369. https://doi.org/10.1007/s12274-014-0501-4
Hu L, Yang Z, Cui L, Li Y, Hao H, Wang Y, Du B (2016) Fabrication of hyperbranched polyamine functionalized graphene for high-efficiency removal of Pb (II) and methylene blue. Chem Eng J 287:545–556
Huang Y, Zeng X, Guo L, Lan J, Zhang L (2018) Heavy metal ion removal of wastewater by zeolite-imidazolate frameworks. Sep Purif Technol 194(462):469
Janusz W, Sydorchuk V, Khalameida ESS, Zięba JS (2022) Adsorption affinity of Zn(II) ions for nanostructured zirconium phosphate/silica or titania composites. Appl Nanosci 12:725–734. https://doi.org/10.1007/s13204-021-01722-w
Jian M, Liu B, Liu R, Qu J, Wang H, Zhang X (2015) Water-based synthesis of zeolitic imidazolate framework-8 with high morphology level at room temperature. RSC Adv 5(60):48433–48441. https://doi.org/10.1039/c5ra04033g
Jin CX, Shang HB (2021) Synthetic methods, properties and controlling roles of synthetic parameters of zeolite imidazole framework-8: a review. J Solid State Chem 297:122040. https://doi.org/10.1016/j.jssc.2021.122040
Kaur H, Mohanta GC, Gupta V, Kukkar D, Tyagi S (2017) Synthesis and characterization of ZIF-8 nanoparticles for controlled release of 6-mercaptopurine drug. J Drug Deliv Sci Technol 41:106–112. https://doi.org/10.1016/j.jddst.2017.07.004
Khan IU, Othman MHD, Ismail AF, Ismail N, Jaafar J, Hashim H, Jilani A (2018) Structural transition from two-dimensional ZIF-L to three-dimensional ZIF-8 nanoparticles in aqueous room temperature synthesis with improved CO2 adsorption. Mater Charact 136:407–416. https://doi.org/10.1016/j.matchar.2018.01.003
Khan A, Toufiq AM, Tariq F, Khan Y, Hussain R, Akhtar N, Rahman URS (2019) Influence of Fe doping on the structural, optical and thermal properties of α-MnO2 nanowires. Mater Res Express 6(6):065043
Kumari P, Alam M, Siddiqi WA (2019) Usage of nanoparticles as adsorbents for waste water treatment: an emerging trend. Sustain Mater Technol 22:e00128. https://doi.org/10.1016/j.susmat.2019.e00128
Li CP, Du M (2011) Role of solvents in coordination supramolecular systems. Chem Commun 47(21):5958–5972. https://doi.org/10.1039/c1cc10935a
Li J, Yi-nan W, Li Z, Zhang B, Zhu M, Hu X, Li F (2014) Zeolitic imidazolate framework-8 with high efficiency in trace arsenate adsorption and removal from water. J Phys Chem 118(47):27382–27387
Li N, Zhou L, Jin X, Owens G, Chen Z (2019) Simultaneous removal of tetracycline and oxytetracycline antibiotics from wastewater using a ZIF-8 metal organic-framework. J Hazard Mater 366:563–572. https://doi.org/10.1016/j.jhazmat.2018.12.047
Li K, Miwornunyuie N, Chen L, Jingyu H, Amaniampong PS, Koomson DA, Lu H (2021) Sustainable application of ZIF-8 for heavy-metal removal in aqueous solutions. Sustainability (switzerland) 13(2):1–11. https://doi.org/10.3390/su13020984
Liao C, Liu Y, Lan X, Jiang X, Liu G, Yu J (2021) Construction of a novel nitrogen- and oxygen-containing GO-based composite with specific adsorption selectivity. J Environ Chem Eng 9:104952. https://doi.org/10.1016/j.jece.2020.104952
Maaloul N, Oulego P, Rendueles M, Ghorbal A, Diaz M (2021) Enhanced Cu(II) adsorption using sodium trimetaphosphate – modified cellulose beads: equilibrium, kinetics, adsorption mechanisms, and reusability. Environ Sci Pollut Res 28:46523–46539
Malekmohammadi M, Fatemi S, Razavian M, Nouralishahi A (2019) A comparative study on ZIF-8 synthesis in aqueous and methanolic solutions: effect of temperature and ligand content. Solid State Sci 91:108–112. https://doi.org/10.1016/j.solidstatesciences.2019.03.022
Mobasherpour I, Salahi E, Pazouki M (2012) Comparative of the removal of Pb2+, Cd2+ and Ni2+ by nano crystallite hydroxyapatite from aqueous solutions: adsorption isotherm study. Arab J Chem 5(4):439–446. https://doi.org/10.1016/j.arabjc.2010.12.022
Moh PY, Brenda M, Anderson MW, Attfield MP (2013) Crystallisation of solvothermally synthesised ZIF-8 investigated at the bulk, single crystal and surface level. CrystEngComm 15:9672–9678. https://doi.org/10.1039/c3ce40943k
Moharana A, Kumar A, Thakur A, Vo D-VN, Sharma AJ, Kumar D (2021) Role of nanostructured metal oxides in photocatalysis: an overview. Nanostructured photocatalysts. Elsevier, Amsterdam, pp 145–167
Moharram MAK, Tohami K, El Hotaby WM, Bakr AM (2016) Graphene oxide porous crosslinked cellulose nanocomposite microspheres for lead removal: kinetic study. React Funct Polym 101:9–19. https://doi.org/10.1016/j.reactfunctpolym.2016.02.001
Mosoarca G, Vancea C, Popa S, Gheju M, Boran S (2020) Syringa vulgaris leaves powder a novel low - cost adsorbent for methylene blue removal: isotherms, kinetics, thermodynamic and optimization by Taguchi method. Sci Rep 10:17676. https://doi.org/10.1038/s41598-020-74819-x
Nasir AM, Md Nordin NAH, Goh PS, Ismail AF (2018) Application of two-dimensional leaf-shaped zeolitic imidazolate framework (2D ZIF-L) as arsenite adsorbent: kinetic, isotherm and mechanism. J Mol Liq 250:269–277. https://doi.org/10.1016/j.molliq.2017.12.005
Navarro-pardo F, Martínez-barrera G, Martínez-hernández AL, Castaño VM, Rivera-armenta JL, Medellín-rodríguez F (2013) Effects on the thermo-mechanical and crystallinity properties of nylon 6,6 electrospun fibres reinforced with one dimensional (1D) and two dimensional (2D) carbon. Materials 6(8):3494–3513. https://doi.org/10.3390/ma6083494
Ourimi HG, Nezhadnaderi M (2020) Comparison of the application of heavy metals adsorption methods from aqueous solutions for development of sustainable environment. Environ Educ Sustain Dev 4(2):15–27. https://doi.org/10.2234/ap.2020.1902797.1066
Pan Y, Liu Y, Zeng G, Zhao L, Lai Z (2011) Rapid synthesis of zeolitic imidazolate framework-8 (ZIF-8) nanocrystals in an aqueous system. Chem Commun 47:2071–2073
Panayotova M, Velikov B (2003) Influence of zeolite transformation in a homoionic form on the removal of some heavy metal ions from wastewater. J Environ Sci Health Part A 38(3):545–554. https://doi.org/10.1081/ESE-120016916
Peng W, Li H, Liu Y, Song S (2017) A review on heavy metal ions adsorption from water by graphene oxide and its composites. J Mol Liq 230:496–504
Pohl A (2020) Removal of heavy metal ions from water and wastewaters by sulfur-containing precipitation agents. Water Air Soil Pollut 231(10):503. https://doi.org/10.1007/s11270-020-04863-w

Pokhrel J, Bhoria N, Anastasiou S, Tsoufis T (2018) CO2 adsorption behavior of amine-functionalized ZIF-8, graphene oxide, and ZIF-8/ graphene oxide composites under dry and wet conditions. Microporous Mesoporous Mater 267:53–67

Schejn A, Balan L, Aranda L, Medjahdi G (2014) Controlling ZIF-8 nano- and microcrystal formation and reactivity through zinc salt variations †. CrystEngComm 16:4493–4500. https://doi.org/10.1039/c3ce42485e

Shahzad A, Miran W, Rasool K, Nawaz M, Jang J, Lim S, Lee DS (2017) Heavy metals removal by EDTA-functionalized chitosan graphene oxide nanocomposites. RSC Adv 7:9764–9771

Shams M, Dehghani MH, Nabizadeh R, Mesdaghinia A, Alimohammadi M, Najafpoor AA (2016) Adsorption of phosphorus from aqueous solution by cubic zeolitic imidazolate framework-8: modeling, mechanical agitation versus sonication. J Mol Liq 224:151–157. https://doi.org/10.1016/j.molliq.2016.09.059

Shanmugaraj K, Campos CH, Viswanathan R (2022) Gold nanoparticle – decorated earth - abundant clay nanotubes as catalyst for the degradation of phenothiazine dyes and reduction of 4-(4-nitrophenyl)morpholine. Environ Sci Pollut Res. https://doi.org/10.1007/s11356-022-19523-1

Shirsath DS, Shirivastava VS (2015) Adsorptive removal of heavy metals by magnetic nanoadsorbent: an equilibrium and thermodynamic study. Appl Nanosci 5:927–935. https://doi.org/10.1007/s13204-014-0390-6

Singh J, Kumar D, Kumar PS, Huerta Aguilar CA, Vo D-VN, Sharma A, Kaur H (2021) Magnetically active Ag–Zn nanoferrites synthesized by solution combustion route: physical chemical studies and density functional theory analysis. Mater Today Chem 22:100588

Song S, Wang K, Zhang Y, Wang Y, Zhang C, Wang X, Wang X (2019) Self-assembly of graphene oxide/PEDOT:PSS nanocomposite as a novel adsorbent for uranium immobilization from wastewater. Environ Pollut 250:196–205. https://doi.org/10.1016/j.envpol.2019.04.020

Thomas M, Illathvalappil R, Kurungot S, Nair BN, Mohamed AP, Anilkumar GM, Hareesh US (2016) Graphene oxide sheathed ZIF-8 microcrystals: engineered precursors of nitrogen-doped porous carbon for efficient oxygen reduction reaction (ORR). ACS Appl Mater Interfaces 8(43):29373–29382

Troyano J, Carne-Sanchez A, Avci C, Imaz I, Maspoch D (2019) Colloidal metal–organic framework particles: the pioneering case of ZIF-8. Chem Soc Rev 48:5534–5546. https://doi.org/10.1039/c9cs00472f

Xu J, Liu C, Hsu PC, Zhao J, Wu T, Tang J, Cui Y (2019) Remediation of heavy metal contaminated soil by asymmetrical alternating current electrochemistry. Nat Commun 10(1):1–8. https://doi.org/10.1038/s41467-019-10472-x

Zhang Y, Jia Y, Li M, Hou L (2018) Influence of the 2-methylimidazole/zinc nitrate hexahydrate molar ratio on the synthesis of zeolitic imidazolate framework-8 crystals at room temperature. Sci Rep 8(1):1–7. https://doi.org/10.1038/s41598-018-28015-7

Zhou Y, Zhou L, Zhang X, Chen Y (2016) Preparation of zeolitic imidazolate framework-8/graphene oxide composites with enhanced VOCs adsorption capacity. Microporous Mesoporous Mater 225:488–493

Zhu B, Xia P, Ho W, Yu J (2015) Isoelectric point and adsorption activity of porous g-C3N4. Appl Surf Sci 344:188–195. https://doi.org/10.1016/j.apsusc.2015.03.086